International Journal of Hyperthermia

ISSN: 0265-6736 (Print) 1464-5157 (Online) Journal homepage: informahealthcare.com/journals/ihyt20

Local moderate magnetically induced hyperthermia using an implant formed in situ in a mouse tumor model

Pol-Edern Le Renard, Franz Buchegger, Alke Petri-Fink, Frederik Bosman, Daniel Rüfenacht, Heinrich Hofmann, Eric Doelker & Olivier Jordan

To cite this article: Pol-Edern Le Renard, Franz Buchegger, Alke Petri-Fink, Frederik Bosman, Daniel Rüfenacht, Heinrich Hofmann, Eric Doelker & Olivier Jordan (2009) Local moderate magnetically induced hyperthermia using an implant formed in situ in a mouse tumor model, International Journal of Hyperthermia, 25:3, 229-239, DOI: 10.1080/02656730802713557

To link to this article: https://doi.org/10.1080/02656730802713557

Int. J. Hyperthermia, May 2009; 25(3): 229–239

informa
healthcare

RESEARCH ARTICLE

Local moderate magnetically induced hyperthermia using an implant formed in situ in a mouse tumor model

POL-EDERN LE RENARD[1], FRANZ BUCHEGGER[2], ALKE PETRI-FINK[3], FREDERIK BOSMAN[4], DANIEL RÜFENACHT[5], HEINRICH HOFMANN[3], ERIC DOELKER[1], & OLIVIER JORDAN[1]

[1]*School of Pharmaceutical Sciences, University of Geneva, University of Lausanne, Geneva,* [2]*Service of Nuclear Medicine, University Hospital of Lausanne, Lausanne, University Hospital of Geneva, Geneva,* [3]*Laboratory for Powder Technology, Ecole Polytechnique Fédérale de Lausanne (EPFL), Lausanne,* [4]*Department of Pathology, University Hospital of Lausanne, Lausanne and* [5]*Neurointerventional Service, University Hospital of Geneva, Geneva, Switzerland*

(Received 6 May 2008; revised 11 December 2008; accepted 27 December 2008)

Abstract

Purpose: We investigate a new heat delivery technique for the local treatment of solid tumors. The technique involves injecting a formulation that solidifies to form an implant in situ. This implant entraps superparamagnetic iron oxide nanoparticles (SPIONs) embedded in silica microbeads for magnetically induced moderate hyperthermia. Particle entrapment prevents phagocytosis and distant migration of SPIONs. The implant can be repeatedly heated by magnetic induction.

Methods: We evaluated heating and treatment efficacies by means of thermometry and survival studies in nude mice carrying subcutaneous human colocarcinomas. At day 1, we injected the formulation into the tumor. At day 2, a single 20-min hyperthermia treatment was delivered by 141-kHz magnetic induction using field strengths of 9 to 12 mT under thermometry.

Results: SPIONs embedded in silica microbeads were effectively confined within the implant at the injection site. Heat-induced necro-apoptosis was assessed by histology on day 3. On average, 12 mT resulted in tumor temperature of 47.8°C, and over 70% tumor necrosis that correlated to the heat dose (AUC = 282°C·min). In contrast, a 9-mT field strength induced tumoral temperature of 40°C (AUC = 131°C·min) without morphologically identifiable necrosis. Survival after treatment with 10.5 or 12 mT fields was significantly improved compared to non-implanted and implanted controls. Median survival times were 27 and 37 days versus 12 and 21 days respectively.

Conclusion: Five of eleven mice (45%) of the 12 mT group survived one year without any tumor recurrence, holding promise for tumor therapy using magnetically induced moderate hyperthermia through injectable implants.

Keywords: *Magnetic induced hyperthermia, superparamagnetic nanoparticles, implant, precipitating polymers, subcutaneous xenograft, necrotizing colocarcinoma, survival, thermometry*

Introduction

Hyperthermia, the therapeutic application of heat, has revealed large benefits in oncology. Moderate hyperthermia (resulting in tissue temperatures of 40° to 46°C) is associated with cytotoxic protein destabilization and denaturation. Cellular defense against heat consists in reactions favoring tolerance to heat stress, closely correlated with the induction of heat

Correspondence: Pol-Edern Le Renard, School of Pharmaceutics and Biopharmaceutics, Geneva University of Science, Quai Ernest-Ansermet, 30, 1221 Geneva 4, Switzerland. Tel: +4122 379 3296. Fax: +4122 379 6567. E-mail: Pol-edern.lerenard@unige.ch

ISSN 0265–6736 print/ISSN 1464–5157 online
DOI: 10.1080/02656730802713557

shock proteins. This tolerance is inhibited above the temperature threshold of about 42°C and the result is in a pronounced increase in cell death rate [1]. Moderate hyperthermia turns the vascular deficiency of a tumor to therapeutic gain by taking advantage of relative enhanced sensitivity to heat damage. A variety of reference therapies in oncology – namely, radiotherapy, brachytherapy, chemotherapy or a combination thereof – have been synergistically combined with moderate hyperthermia [2, 3].

The outcome of a hyperthermia treatment correlates to the heat dose administered [4], which, in turn, is dependent upon anatomical situation and heating modalities. Local hyperthermia aims to confine heat delivery to the lesion site. Despite steady improvements in heating localization of external or interstitial modalities based on standard heat application means (radiofrequencies, microwaves and ultrasounds), physical limitations still hinder the treatment of deep-seated lesions [5]. Power transmission in the case of acoustic or electromagnetic waves is limited by the reflection and absorption of power into tissue and interstitial liquid. In contrast, magnetic fields can cross the diamagnetic body of a patient without losses. Monodisperse superparamagnetic iron oxide nanoparticles (SPIONs) exposed to alternative magnetic fields (AMFs) convert the magnetization energy into heat. This scales as $P \propto H^2 f^2$ where P is the power loss, H the AMF amplitude and f the frequency [6, 7]. The rate of heat generation is larger than for metallic implant such as seed [8]. Magnetic fluid hyperthermia [9], i.e. heating interstitially injected SPIONs through alternating magnetic induction, has also shown promising clinical results [10–13]. One drawback of current administration techniques is that SPIONs fade ineluctably out from the injection site into the lymphatic and blood circulation or are sequestrated in macrophage, exposing patient to potentially toxic hazards [14].

We report here the feasibility of an original approach of magnetically induced local moderate hyperthermia through an in situ-formed implant that traps SPIONs embedded in silica microbeads. After injection in aqueous environment and precipitation from their organic solvent formulation, water-insoluble polymer chains entangle and form a matrix holding the dispersed superparmagnetic microbeads. SPIONs are hence protected and durably confined at the injection site, avoiding their phagocytosis and distant migration. The opportunity to repeat implant heating in the long term as necessary could also offer therapeutic benefits. We performed thermometry and survival studies in a model of human colocarcinoma tumor that was subcutaneously engrafted in nude mice. Our goal was to assess heating efficiency and treatment potential of local moderate magnetically induced hyperthermia delivered through the implant formed in situ.

Materials and methods

Magnetics beads

We used silica particles containing 32% w/w of nanometric iron oxide particles of 10-nm mean diameter. The micron-sized particles had a density of $2.12 \pm 0.02\,\mathrm{g{\cdot}cm^{-3}}$ at 25°C. They were synthesized as described by Chastellain et al. [15]. Briefly, tetramethoxysilane (45 mL) was added to a 2 M solution of $Fe(NO_3)_3 \cdot 9H_2O$ in ethanol (44.4 g iron salt in 55 mL ethanol). The mixture was stirred vigorously for 10 min, transferred to a sealed glass container and allowed to gel at 50°C. The obtained brown gel was ground and separated by sieving. Particles smaller than 100 μm were thermally treated at 500°C for 24 h, followed by high-energy attrition milling for 1 h. Measurements using a superconducting quantum interference device (SQUID) confirmed superparamagnetic properties. The specific absorption ratio (SAR), which reflects the heating capacities, is conventionally defined as the slope of the initial temperature rise multiplied by the specific heat capacity. In our case, this was in the order of 18 W/g iron oxide for a 12-mT magnetic field. The volume median diameter of the silica beads containing the iron oxide was determined on a Malvern Mastersizer as $(D(v, 0.5)) = 0.9\,\mu m$. The sizes of the magnetic iron oxide nanoparticles as established by transmission electron microscopy (TEM), X-ray diffraction (XRD), and zero-field cooled magnetic measurements were 9 ± 1 nm, 11.3 ± 1 nm and 15.5 ± 1.3 nm, respectively.

Injectable formulation

The ethylene vinyl alcohol copolymer EVAL™ 105-B (EVAL Europe, Zwijndrecht, Belgium) was dissolved at 8% (w/v) in pharmaceutical grade dimethyl sulfoxide (DMSO) (Gaylord Chemical Corp., Los Angeles). Using ultrasound and vigorous mechanical stirring, the beads were suspended at 40% (w/v) in the resulting polymer solution. The preparation was finally sterilized by 15 min autoclaving at 121°C. As flocculated sedimentation occurred during storage, energetic shaking restored suspension homogeneity before use. Based on pycnometric measurements and calculations, the resulting density of the formulation was in the order of $1.26\,\mathrm{g{\cdot}cm^{-3}}$.

Alternating magnetic field generator

The field generator used (TIG 2.5, Hüttinger Elektronik, Freiburg, Germany) consisted of an alternating current generator feeding the coil inductor (internal, external diameters and length of the horizontal coil were 54, 64 and 46 mm respectively). A conical tube mouse restrainer was introduced within the coil so that the implanted tumor was positioned at the center. With a small pick-up coil calibrated using a teslameter we found a linear relationship between the magnetic field amplitude at 141 kHz and the generator peak-to-peak voltage. Current intensity was adjusted to impose the voltage corresponding to the chosen field strength.

Tumor model

Tumors generated by subcutaneous injection of the human Co112 colon carcinoma cells were maintained by serial subcutaneous transplantation in Swiss nude mice [16]. About 15 mm^3 of excised and minced tumor was subcutaneously engrafted into the right flank of 5-week-old Swiss nude mice and the nodule was allowed to grow for 4 to 6 weeks. We determined the volume of the tumor (V_{tum}) by measuring with calipers three tumor dimensions: length (l), width (w) and thickness (t) and using the following formula: $V_{tum} = \frac{1}{2}(lwt)$ [17], with an uncertainty of $\pm 15\%$. Care was taken to implant the tumor above hind leg musculature in order to avoid detrimental heat exposure of intestinal tissues. The obtained tumor showed peripheral angiogenesis, necrosis in the tumor center core and a pseudocapsule composed of connective tissue. Central necrosis is a common feature in Co112 tumors, also observed in in vitro-grown multicellular spheroids and liver metastases [18].

Mice

One-month-old female Swiss nude mice were supplied by Charles Rivers (Iffa Credo, Saint Germain sur l'Arbresle, France). Animal experiments were performed according to the ethical principles of laboratory animal care and Swiss legislation. Experiments were specifically approved by the official committee of animal research surveillance of the local authority. Animals were maintained in SPF animal house under a 12 h light and 12 h darkness cycle with normal diet, ad libitum, respecting a maximum of five animals per cage. Animals were euthanized by asphyxia under CO_2 saturated atmosphere.

Implantation

We set the injection volume to 0.25 mL (i.e. 84.1 mg of magnetic microparticles or 26.9 mg of iron oxide) to ensure that the intra-tumoral implant mass would be sufficiently large to heat the entire tumor. This injection volume was as large as or slightly larger than the tumor volume. The DMSO dose injected was below the mouse intraperitoneal LD_{50} (13 g/kg) [19]. The formulation was slowly injected over a 1-2 min period into the tumor through a 22G needle. Systemic and local toxicities were limited. Thanks to the brownish color and stiffness of the implant, we could manage and verify correct implant distribution by observing tissue darkening and induration. The implant first entered into the necrotic core and then extended towards the surrounding pseudocapsule to reach the peripheral border of the tumor. To avoid distant leakage, we paid special attention to needle positioning, in order to distribute the implant uniformly without accumulation in a part of the nodule. The procedure gave rise only to transient perinodular edema, which was spontaneously resorbed by the time we proceeded to alternating magnetic field stimulation.

Thermometry

We monitored temperature with a fluoroptic thermometer (Luxtron, Santa Clara, CA) using three fiber optic probes of 200 μm diameter. The device reported temperatures once a second with 0.1°C accuracy. A one-point calibration at 20.0°C was performed before each experiment. Data were acquired using Physitemp software (Luxtron).

In vivo *investigation protocols*

Thermometry studies: 0.25 mL of the 8% (w/v) EVAL solution in DMSO containing 40% (w/v) microbeads was injected into each mouse tumor (day 1). After 24 h, the animal was exposed to a 20-min alternating magnetic field (141 kHz), under halothane-induced general anesthesia (day 2). We investigated five magnetic field strengths: 9, 10, 10.5, 11 and 12 mT with respectively $n = 5$, 3, 6, 3 and 5 animals per group. Temperatures were monitored in the tumor, on the skin over the tumor, and in the hollow of the brachial plexus. The animals were sacrificed 24 h later (day 3) for standard histology. Tumor size in the animals used for thermometry studies was in the range of 0.1 to 0.3 cm^3.

Survival studies: For the survival investigation protocol, we injected 0.25 mL of 8% (w/v) EVAL solution in DMSO containing 40% (w/v) beads (day 1). After 24 h, animals were exposed to an alternating magnetic field (141 kHz) for 20 min (day 2). Two thermometry probes were affixed to the skin over the tumor, and one was fixed over the brachial plexus. Animals were sacrificed when the

tumor volume reached ten times the initial volume. We investigated four groups: control with neither implant nor magnetic field ($n=6$), implanted control (no magnetic field) ($n=7$), 10.5 mT treated ($n=7$), and 12 mT treated ($n=11$). Animals were assigned to different treatment and control groups in order to ensure similar mean tumor sizes: the respective mean initial tumor size and standard deviations were 59 ($\pm$54) mm^3 for the control group, 52 ($\pm$44) mm^3 for the implanted control group, 53 ($\pm$33) mm^3 for the 10.5-mT treated group and 64 ($\pm$42) mm^3 for the 12-mT treated group. In a multigroup comparison, tumor size in the different groups was indeed shown to be very similar (Friedman test: $p>0.8$).

Histology

The tumors and part of the surrounding tissues (overlying skin and adjacent muscle fascia or peritoneum) were fixed in buffered neutral formalin (1 : 10). Slices 3 mm thick were embedded in paraffin (through alcohol dehydration and xylol clearing), and 5 µm thick sections were stained with hematoxylin and eosin. The ratio of necrotic tumor to whole tumor volume was semi-quantitatively scored from 0 to 100%. Microphotography was performed with a Nikon eclipse E800 microscope (Olympus Corp., Center Valley, USA) and histomorphometry using ImageJ 1.38x software (National Institutes of Health, USA).

Imaging

For magnetic resonance imaging we used a MRI scanner (Achieva 1.5T, Philips, Eindhoven, the Netherlands). For micro-computerized tomography, we used a Micro-CT scanner (Skyscan 1076, Kontich, Belgium).

Statistics

StatView version 5.0 software (© SAS Institute Inc.) was used for statistical analysis. Statistical significance was considered at $p<0.05$. For the thermometry study we used the Kruskall-Wallis test, the Mann-Whitney U test and the Spearman correlation test. For the survival studies we employed the Friedman test and Kaplan Meyer analysis.

Results

Precipitation of the injectable formulation fills the initially necrotic core and peripheral extensions of the tumor

Injection of the formulation was accompanied by mild acute toxicity [20, 21]. The injected 0.25-mL volume in a 25-g mouse would translate to 700 mL in a 70-kg patient, representing indeed a large injection volume per body weight. Systemic manifestations, most probably due to DMSO, consisted of transient fatigue and ocular irritation with eyelid ptosis. Locally, we observed edematous dilatation of the tumor site. Edema was rapidly reversed along with solvent clearance. Afterwards, the implanted tumor when recovered was shown to have dimensions larger than the initial tumor.

As previously observed in other experiments, Co122 tumors showed extensive central necrosis (up to 50%) [22]. Similar necrotic centers have been observed in Co112 multicellular spheroids grown in vitro [23]. Under electron microscopy, the Co112 tumor spheroids developed junctional complexes and desmosomes, while oxygen measurements had shown severe central hypoxia [24]. Histology confirmed that the implant was invariably present in the necrotic tumor core and extended towards the viable peripheral rim of cells. We did not observe an inflammatory response in either the control or the implanted control groups, sacrificed one day after injection (Figure 2a). Occasionally an implant extension had leaked into peritumoral loose connective tissue, mostly in the case of small and vital tumors. To assess implant distribution, we quantified the percentage of the implant that was in contact with stromal tissue (Table I) and found correlation only with the initial tumor volume (Spearman $\rho=0.645$; $p=0.0412$), not with thermometry parameters.

Entrapment of microbeads within the implant polymer network was confirmed through use of the Prussian Blue stain, which identified iron

Table I. Summary of parameters (mean $\pm$ SD) calculated for each group of the thermometry study for 5 magnetic field strengths.

Field strength (mT)	9 ($n=5$)	10 ($n=3$)	10.5 ($n=6$)	11 ($n=3$)	12 ($n=5$)
Initial tumor volume (mm^3)	217 ± 254	122 ± 38	119 ± 82	279 ± 60	220 ± 104
Implant that is in contact with stromal tissues (%)	67 ± 39	55 ± 38	72 ± 12	60 ± 30	50 ± 19
Tumor ET (°C)	$40.0\pm3.1^{\star}$	42.5 ± 3.7	$42.9\pm2.3^{\S}$	$43.5\pm1.6^{\dagger}$	$47.8\pm2.2^{\star\S\dagger}$
Tumor AUC (°C·min)	$131.1\pm44.3^{\star}$	$168.8\pm47.8^{\S}$	$183.4\pm39.9^{\dagger}$	$183.8\pm34.0^{\|}$	$282.5\pm40.0^{\star\S\dagger\|}$
Skin ET (°C)	$38.6\pm3.0^{\star\dagger}$	42.4 ± 4.0	$42.0\pm2.0^{\S\dagger}$	$43.5\pm2.0^{\|}$	$48.4\pm2.0^{\star\S\|}$
Tumor necrosis (%)	67 ± 25	56 ± 15	60 ± 25	52 ± 13	78 ± 6

The U Mann-Withney test was used to evaluate statistical significance between the groups of mice. $^{\star}p<0.001$, $^{\S\dagger\|}p<0.05$.

oxide nanoparticles. In vitro, bare SPIONs of nanoscale size were also efficiently trapped by this network. A preliminary formulation study with a batch of finer sub-micrometer beads confirmed entrapment efficiency but resulted in poor syringeability and an inadequate implant distribution pattern.

The implant formed in situ can heat the tumor by magnetic induction at 141 kHz across the whole temperature range of moderate hyperthermia as a function of field strength

Thermograms consistently exhibited a similar shape (Figure 1a). After a steep increase during the first 5 min, temperatures reached a plateau corresponding to an equilibrium between implant heat production and dissipation through diffusion and convection. The observed plateau temperature was not due to a diminishing response capacity of the superparamagnetic beads, since stepwise field increase in a separate experiment had produced stepwise increasing temperatures throughout the 25-min exposure period (Figure 1b). To obtain a parametric value of this equilibrium, we defined the equilibrium temperature (ET) as the averaged temperature over the final 15 min of magnetic field application. Table I shows that the mean tumor site ET increased with magnetic field strength (Spearman $\rho = 0.724$; $p < 0.001$). We observed the lowest mean tumor site ET (40°C) for the group treated with the lowest magnetic field strength, i.e. 9 mT (Table I). Treatments with intermediate magnetic field strengths of 10 to 11 mT led to intermediate mean

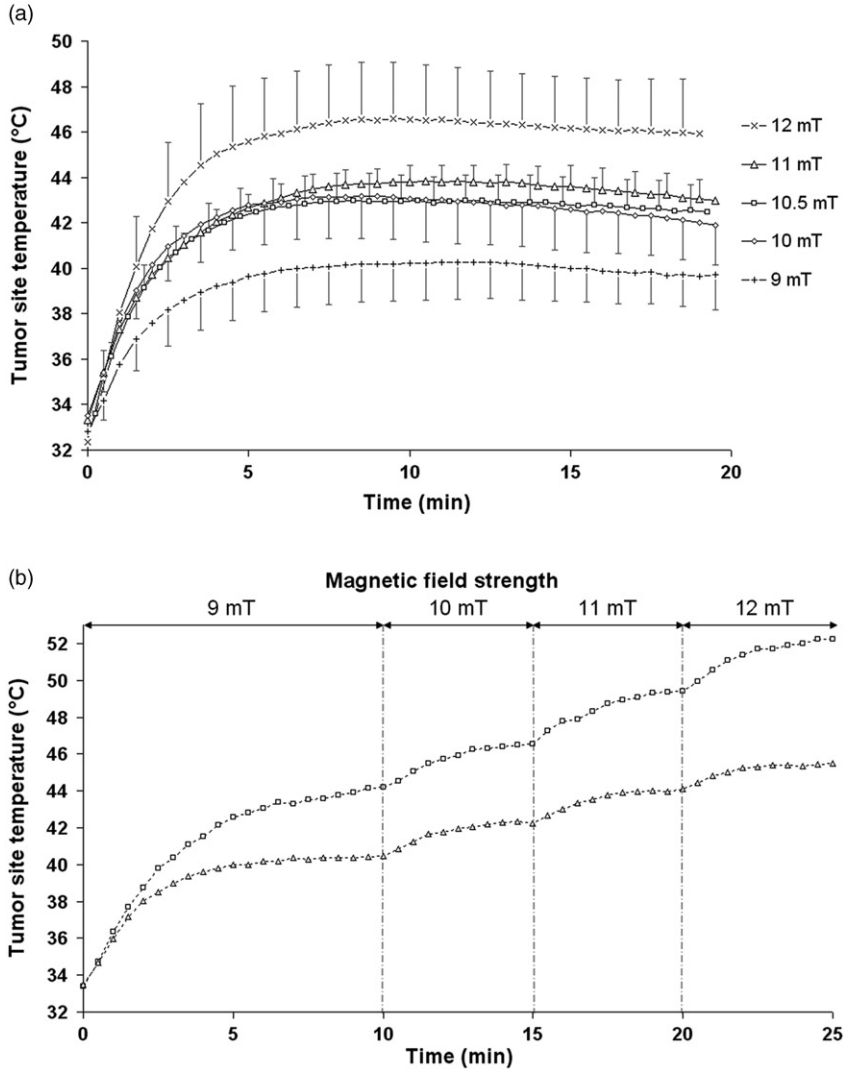

Figure 1. Thermograms representing tumor temperature as a function of time. (a), during single 20-min treatments in a 141 KHz alternating magnetic field, for magnetic field strengths of 9 mT ($n = 5$), 10 mT ($n = 4$), 10.5 mT ($n = 5$), 11 mT ($n = 3$), 12 mT ($n = 5$). (b), during two stepwise 25-min treatments in an 141-KHz alternating magnetic field. Magnetic field strength was 9 mT from 0 to 10 min, 10 mT from 10 to 15 min, 11 mT from 15 to 20 min, 12 mT from 20 to 25 min.

values of tumor site ET between 42.5 to 43.5°C that were not statistically different. For the group treated with 12-mT magnetic field, the mean tumor site ET of 47.8°C was significantly larger than for all other magnetic field strengths.

The area under the curve (AUC) of temperature as a function of time is a parameter related to the heat dose delivered during a given treatment [25, 26]. For the group treated with the highest magnetic field strength (12 mT), we recorded a more than two-fold increase in mean AUC (282.5°C·min) as compared to the group treated with 9 mT (131.1°C min). Mean AUCs for intermediate magnetic field strengths of 10 to 11 mT were again intermediate (Table I). When considering the entire range of investigated magnetic field strengths, AUC was positively correlated with the 5 different magnetic field strengths applied (Spearman $\rho = 0.739$; $p < 0.001$).

Above a threshold temperature, a larger delivered heat dose increases the extent of induced necro-apoptosis to whole tumor

The necrosis to tissue ratio, as quantified using histology, was not significantly different between injected and non-injected controls, suggesting that the implant itself does not induce necrosis. We assessed the heating efficiency microscopically in terms of coagulation necrosis of vital tumor and adjacent tissues. In the case of low heat delivery, the extent of spontaneous and heat-induced necrosis

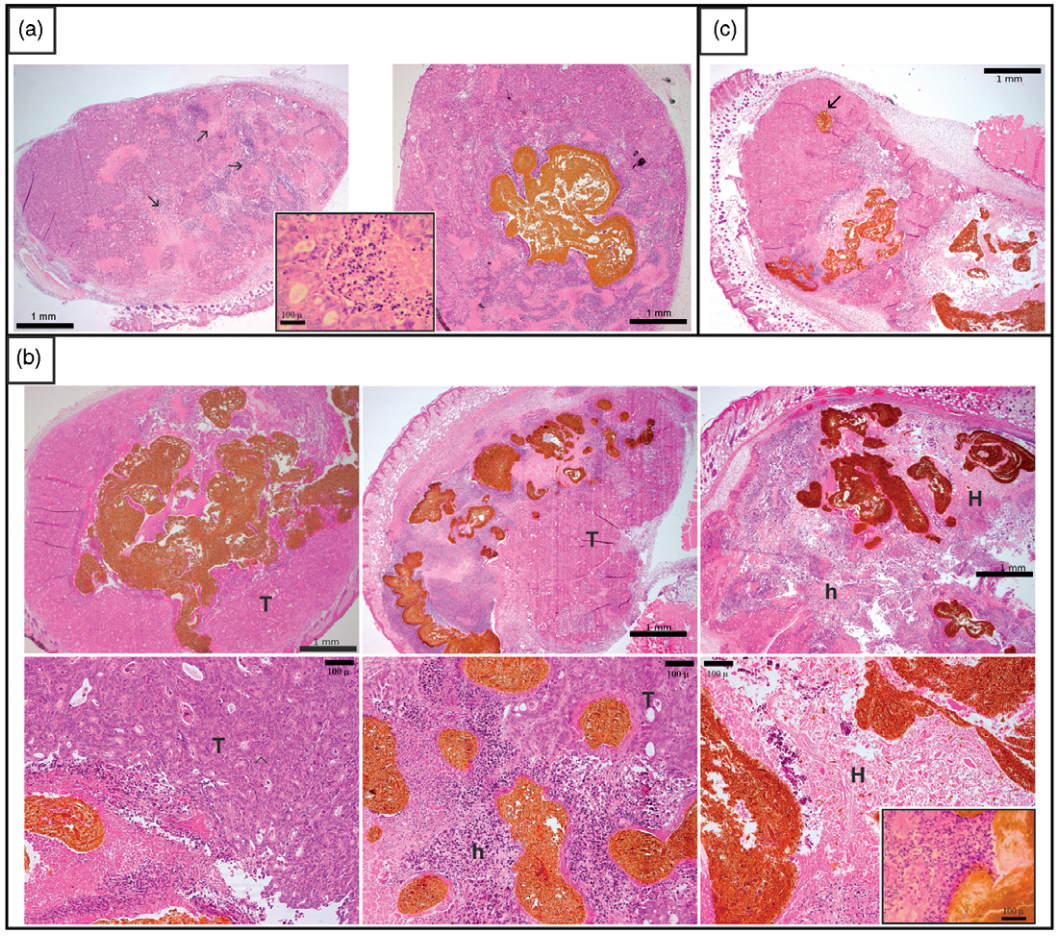

Figure 2. Microphotographs at D2 (with or without implant injection at D0 and hyperthermic treatment at D1). Panel (a) shows at left the control Co112 tumor, with non-induced necrosis (arrow) that typicaliy did not exhibit an inflammatory reaction (insert), and at right the control with the nonheated implant shown in brown. Panel (b) displays three treated tumors at low magnification in the upper row and at higher magnification in the lower row. On the left, a tumor treated with a magnetic field strength of 10 mT (MET = 39.5°C, AUC = 152.8°C1 min) leaving most of viable tumor tissue (T) without any heat-induced necrosis. In the middle, a tumor treated with a magnetic field strength of 10.5 mT (MET = 44.0°C, AUC = 211.8°C1 min) shows clear heat-induced necrosis (h) around the implant, but more distant tumor tissue remains viable. On the right, a tumor treated with a magnetic field strength of 12 mT (MET = 46.2°C, AUC = 284.3°C1 min) illustrates heat induced necrosis (h) covering most of the tumor and effecting intense thermal damage (H) in the vicinity of implant, accompanied by an inflammatory reaction (neutrophils and macrophages, see insert). Panel (c) illustrates the topographic association between implant and heat-induced necrosis. A small isolated extension of the implant (arrow) did not trigger heat damage, in contrast to the more voluminous main body of the implant.

overlapped. However, the extent of the necrosis was quite different between moderately and intensively heated tumors. Figure 2b shows heat-induced damage patterns for three tumors treated at magnetic field strengths of 10, 10.5 and 12 mT, respectively. For treatments associated with temperature higher than 44°C we observed extensive tumor necrosis and coagulation necrosis. In the vicinity of the implant, we observed an inflammatory infiltrate of neutrophils and macrophages as part of non-specific immune response to necrosis. Focal necrosis of the immediately adjacent connective and muscle tissues can be attributed to heat, since this was absent in mice injected with implant alone or at lower heating levels. Likewise, the skin, especially over the implanted tumor, showed heat-induced necrosis. In some animals, muscle tissue at the peritoneal side of the tumor showed signs of thermal damage. For treatments reaching less than 42°C, no significant heat-induced necrosis was observed. Notably, heat-induced necrosis was not observed in implanted mice exposed to the magnetic field strength of 9 mT and was only occasionally found in mice exposed to 10 or 10.5 mT, clearly depending on heating intensity. It was found that AUC was well correlated with heating efficiency at the tissue level, quantified in terms of the percentage of tumor necrosis (Spearman $\rho = 0.468$; $p < 0.05$).

Magnetically induced heat delivery through an implant is highly efficient in treating solid tumor for a magnetic field strength of 12 mT

In groups of animals matched for tumor size, magnetically induced heating of the implant prolonged survival time as defined by growing to 10 times the initial tumor size. After a single 20-min treatment, a median survival time of 27 days was observed for the group treated with a magnetic field strength of 10.5 mT (Figure 3). Median survival time increased further to 37 days for mice treated with 12 mT, as compared with 12 days for non-implanted controls and 21 days for implanted controls. Finally, only one complete response was observed in the 10.5 mT group, while 5 of 11 animals (45%) treated with 12 mT exhibited complete responses that persisted until the one-year mark, when mice were sacrificed. Kaplan-Meyer analysis revealed significant differences between the 10.5-mT treated group and the non-implanted control group ($p < 0.05$), while the 12-mT treated group was significantly different when compared to the implanted and non-implanted controls ($p < 0.05$ and $p < 0.01$, respectively).

Computerized tomography allows for precise implant imaging

We studied implant precipitation pattern in vivo using magnetic resonance imaging (MRI) and computerized tomography (CT) of two implanted and non-treated mice. In MRI, silica-embedded SPIONS led to a susceptibility artifact, partially masking the implanted tumor (Figure 4a). We confirmed entrapment of the beads at the injection site through the absence of distant artifacts. In contrast, micro-computerized tomography allowed detailed imaging of the implant, confirming intra-tumor precipitation pattern of the implant (Figure 4b). Image contrast was set in the bone density range to ensure proper imaging of the high-density implant, albeit masking soft tissues.

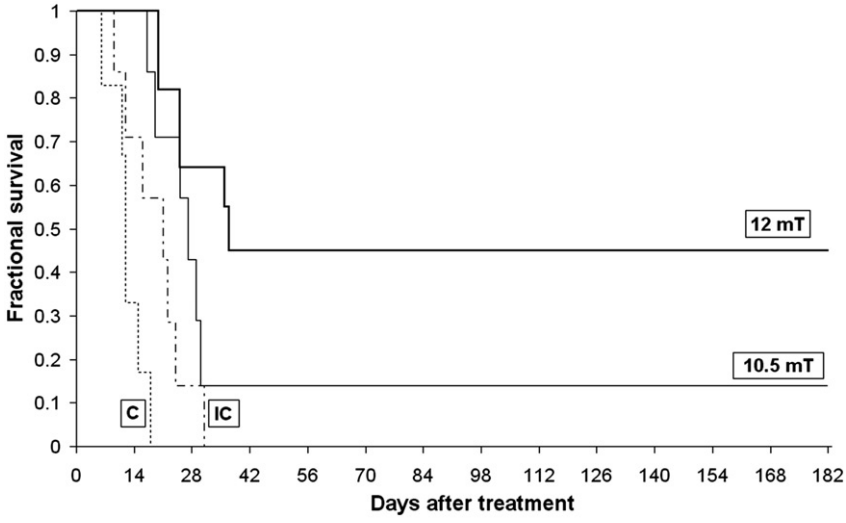

Figure 3. Survival curves. Dotted line: control group (c), $n = 6$; dashed line: implanted control group (IC), $n = 7$ normal line: 10.5-mT treated group, $n = 7$; bold line 12-mT treated group, $n = 11$. Note that in the group treated with a 12-mT alternating magnetic field, 5 of 11 mice survived 12 months after treatment without tumor relapse.

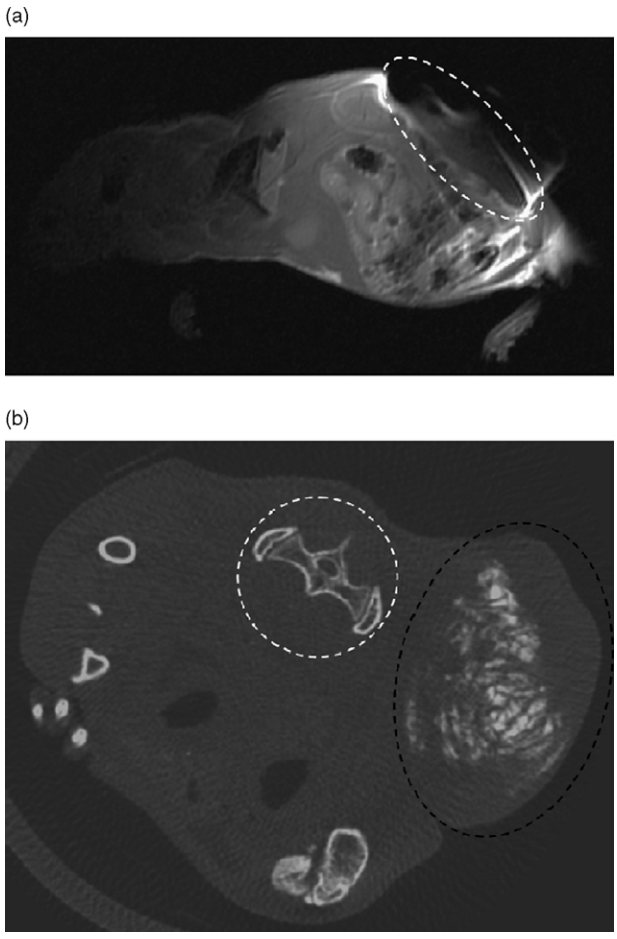

Figure 4. Implant imaging. (a), MRI imaging of a swiss nude mouse bearing a subcutaneous tumor injected with 0.25 ml of the implant formulation, with a T1 weighted sequence. The tumor zone is enclosed in the dotted white circle, highlighting the susceptibility artifact caused by SPION entrapped in the implant. (b), Micro-computerized tomography of a swiss nude mouse bearing a subcutaneous tumor punctured with 0.25 ml of the implant formulation. In the transversal, section, we can precisely localize the implant (in white) and the tumor that is enclosed within the dotted black circle. The SPIONs entrapped in the implant allowed for X-ray absorption with an absorption density close to that of bone (see, for instance, the spinal vertebrae and iliac wing highlighted by the dotted white circle). Note that the window is adjusted for bone density without further soft tissue contrast refinements or the use of contrast agent.

Randomly distributed density measurements ($n = 100$) recorded in the implant volume suggested a relatively homogeneous iron distribution, with a variation coefficient of 10% over the whole implant.

Discussion

Our results show the feasibility of implant-mediated hyperthermia using an injected formulation of superparamagnetic beads that solidifies upon contact with interstitial fluid.

A gradual injection gave sufficient time for the formulation to spread into the tumor before subsequent precipitation and solid implant formation in situ. The tumor necrotic center was initially filled, and the precipitation subsequently extended towards the peripheral tumor spaces. Although attractive, the concept of an implant layer in contact with the outer tumor rim, where vital cancer cells are found, seems impractical due to the dense heterogeneous tissue surrounding the tumor core. In the absence of image guidance, tumor core injection led to a more controlled implantation. This last step was critical with regard to eventual occurrence of leakage. The implant volume was constrained in situ to match the tumor volume. The injection volume of 0.25 mL was acceptable even if it was larger than initial tumor volume. This is partly explained by implant mass loss following diffusion and exchange of DMSO with water (~16%), and partly by tumor distension following implantation and edema resorption. Similar formulations without magnetic particle have shown in preliminary ex vivo experiments [27], that implant volume was constant in situ and that the DMSO solvent most likely induced tissue swelling. Noteworthy, the resulting viscoelasticity of such formulation, as in the case of bone cements, can lead to overestimation of the injected volume due to contraction. This can also be associated with needle withdrawal before complete flow arrests, as well as with compositional variations following filtration through reversible particle aggregates [28, 29]. The implant was localized at the center of the tumor but it did extend into peripheral layers. This was particularly appropriate for magnetically induced delivery of heat produced by the entrapped superparamagnetic micron-sized particles. This entrapment was very efficacious and we never observed particles outside the tumor volume under multiple orthogonal techniques (histology, CT and MRI). We also attempted to use smaller particles, including sub-micrometer silica beads and 20-nm bare SPIONs. We observed efficient entrapment in the precipitated polymer network, but, with these smaller beads, the preparation resulted in rheological behavior that was prone to leakage.

In a clinical scenario, the application of AMF could lead to safety concerns. The side effects of AMF can include non-specific heating outside the target volume due to the magnetic induction of current density called eddy currents (EC) [30]. More problematic is the case of radiofrequencies [31], for which adverse excitation of neurons can be easily triggered by induced electric fields. Heat produced by EC, scaled as: $SAR_{EC} \propto (H \cdot f)^2 r^2$, where SAR is the specific absorption rate (W/g tissue), and r is the

radius of exposed region [32], can lead to distant painful hot spots that would limit the values of f and H, and thus the heating possibilities. The AMF used here is associated with $(H \cdot f)$ values ranging from $10{\cdot}10^8$ to $13.5{\cdot}10^8$ A/(m·s) for 9 mT (7.2 kA/m) and 12 mT (9.6 kA/m), at 141 kHz. These fields did not induce any directly measurable effect in control mice that had not received any implant. Accordingly, we believe that this approach would be entirely appropriate for human [33]. In the case of AMF treatment of prostate cancer, the pelvic skin fold is at particular risk of hot spot triggered by EC. However values of $(H \cdot f)$ up to $5{\cdot}10^8$ A/(m·s) were safe for 100% of the patients [34, 35]. As for AMF treatment of glioblastomas, no side effects were reported during skull exposition for $(H \cdot f)$ values up to $13.5{\cdot}10^8$ A/(m·s) [36]. $(H \cdot f)$ values higher than $20{\cdot}10^8$ A/m/s have been used *in* and ex vivo [37, 38]. Pulses of very high amplitude have been experimentally used in mice [32].

The investigated 9- to 12-mT field strengths induced a tissue temperature rise from mild hyperthermia in the range of 39–42°C extending to cytotoxic moderate hyperthermia in the range of 42–48°C. Treatments at higher temperatures were associated with extensive tumor necrosis and collateral damage mainly to adjacent skin. It is worth mentioning that the tissue origin is of importance: mouse tissues are more sensitive to heat than the human tissues used here in form of the human tumor transplant.

Under alternating magnetic field induction, the measured skin temperatures were generally less than intra-tumor temperatures, so long as heating remained at non-toxic levels. However, on reaching toxic heat levels, the skin temperature rose to intratumoral levels (see Table I). These observations underline the importance of cooling by tissue perfusion [39, 40]. When skin blood perfusion breaks down as a consequence of heat damage to the vasculature, the cooling effect of blood perfusion stops and skin temperature raises to a value close to the tumor temperature.

The extent of heat-induced necrosis seemed to be related to the manner of implant distribution in situ. Thus, around extensions that were confluent or of large cross-section, necrosis was wider than around thin implant extensions (Figure 2c). It is likely that the latter delivered less heat to surrounding tissues [41]. Certainly, this could result from a combination of different factors: first, a threshold mass for dissipating significant heat [42] from the implant center to distant tissue areas, and, secondly, a differential effectiveness in vascular cooling [43]. Indeed, since cooling efficiency is directly related to the contact area between implant and tissue, whereas heating power is proportional to implant mass, small implants that present a higher surface/mass ratio will be more efficiently cooled. Measurement of the necrosis rim width in biologically relevant implants as well as in vitro or in vivo thermal mapping studies indicated a necrosis extent in the order of 2–3 mm, compatible with previously published observations [44].

Our survival study revealed an important therapeutic potential for a single 20-min treatment based on the sole cytotoxicity of hyperthermia. We observed a minor growth delay in the group that received the implant but was not submitted to magnetically induced heating. Although we cannot fully exclude local toxicity of DMSO, this growth delay is more likely due to implant precipitation in capillaries and secondary hemostasis, leading to antineoplastic effects through hypoxia. Magnetically induced hyperthermia treatment, however, did increase significantly the median survival time. A number of definitive complete responses were observed at a rate that depended on the magnetic field amplitude. It is well known that temperature distribution in tumor is essential to assessing treatment responses [45]. This distribution is directly related to magnetic field strength and implant localization, and its control depends on thermometry data. The suboptimal heating of peripheral tumor cells allows for a tumor relapse when tissue escapes the cytotoxic area of the temperature gradient. In comparison to the 10.5-mT single 20-min treatment, these considerations suggest that one might achieve a better outcome by increasing the magnetic field strength to 12 mT.

A survival study using imaging techniques could address the important issue of implant distribution. It would allow controlled injection of the implant and, if necessary, exact localization of thermometry probes. Clinically, imaging could allow a control of the correct implant size and localization to further improve or predict heat delivery. While MRI appeared most sensitive to the presence of the superparamagnetic beads, leading locally to some artifacts, CT was most appropriate for implant imaging without any obvious artifacts in its vicinity. Furthermore, soft tissue contrast agent would allow studies of intratumoral implant distribution.

Regarding the implant durability, we retrieved intact implants as expected at day 14, but we observed partial degradation at day 48 in two treated mice. No implant or tumor was macroscopically observable after the one year survival period. These sparse data points suggest that unexpected degradation occurs after a few months. The high solid fraction may account for loss of implant strength, and the heating process may accelerate focal inflammatory events. These observations warrant further investigations into the distribution and metabolism

pathways of iron in the implants, compared to SPIONs, free or embedded in silica beads.

In conclusion, these results demonstrate the efficacy of superparamagnetic particles embedded in an in situ formed implant to deliver thermal energy in a therapeutically relevant range [46]. Sustained moderate hyperthermia at clinically relevant field strengths were produced in a necrotizing tumor model, holding promise for implant-mediated local hyperthermia therapy.

Acknowledgements

Grant support: Swiss National Science Foundation (grant 3200B0-104508), Switzerland. For histology processing, we are thankful to Susana Leuba, Department of Pathology, Hospital University of Lausanne, Switzerland. We also thank Xavier Montet of the Radio-diagnostic Service, University Hospital of Geneva, Switzerland for MRI and micro-computerized tomography imaging support. We wish to thank Frances Godson of the Radio-oncology Service, University Hospital of Lausanne, Switzerland for manuscript proof reading.

Declaration of interest: The authors report no conflicts of interest. The authors alone are responsible for the content and writing of the paper.

References

1. Hildebrandt B, Wust P, Ahlers O, Dieing A, Sreenivasa G, Kerner T, Felix R, Riess H. The cellular and molecular basis of hyperthermia. Crit Rev Oncol Hematol 2002;43:33–56.
2. Hand JW, Streffer C, van Beuningen D, Vaupel P, Kallinowski F, Molls M, Scherer E, Engelhardt R. Hyperthermia and the Therapy of Malignant Tumors. Berlin: Springer-Verlag; 1987.
3. Falk MH, Issels RD. Hyperthermia in oncology. Int J Hyperthermia 2001;17:1–18.
4. Dewhirst MW, Viglianti BL, Lora-Michiels M, Hanson M, Hoopes PJ. Basic principles of thermal dosimetry and thermal thresholds for tissue damage form hyperthermia. Int J Hyperthermia 2003;19:267–294.
5. Sapozink MD, Corry PM, Kapp DS, Myerson RJ, Dewhirst MW, Emami B, Herman T, Prionas S, Ryan T, Samulski T, et al. RTOG Quality assurance guidelines for clinical trials using hyperthermia for deep-seated malignancy. Int J Radiat Oncol Biol Phys 1991;20:1109–1115.
6. Rosensweig RE. Heating magnetic fluid with alternating magnetic field. J Magn Magn Mater 2002;252:370–374.
7. Wang XM, Gu HC, Yang ZQ. The heating effect of magnetic fluids in an alternating magnetic field. J Magn Magn Mater 2005;293:334–340.
8. Jordan A, Wust P, Fahling H, John W, Hinz A, Felix R. Inductive heating of ferrimagnetic particles and magnetic fluids – Physical evaluation of their potential for hyperthermia. Int J Hyperthermia 1993;9:51–68.
9. Jordan A, Scholz R, Wust P, Fahling H, Felix R. Magnetic fluid hyperthermia. In: Hafeli U, Schütt W, Teller J, and Zborowski M, editors. Scientific and Clinical Applications of Magnetic Carriers. New York: Plenum Press; 1997. pp 569–595.
10. Johannsen M, Gneveckow U, Thiesen B, Taymoorian K, Cho CH, Waldofner N, Scholz R, Jordan A, Loening SA, Wust P. Thermotherapy of prostate cancer using magnetic nanoparticles: Feasibility, imaging, and three-dimensional temperature distribution. Eur Urol 2006;52: 1653–1662.
11. Wust P, Gneveckow U, Johannsen M, Bohmer D, Henkel T, Kahmann F, Sehouli J, Felix R, Ricke J, Jordan A. Magnetic nanoparticles for interstitial thermotherapy—feasibility, tolerance and achieved temperatures. Int J Hyperthermia 2006; 22:673–685.
12. Johannsen M, Gneveckow U, Taymoorian K, Thiesen B, Waldofner N, Scholz R, Jung K, Jordan A, Wust P, Loening SA. Morbidity and quality of life during thermotherapy using magnetic nanoparticles in locally recurrent prostate cancer: Results of a prospective phase I trial. Int J Hyperthermia 2007;23:315–323.
13. Maier-Hauff K, Rothe R, Scholz R, Gneveckow U, Wust P, Thiesen B, Feussner A, von Deimling A, Waldoefner N, Felix R, et al. Intracranial thermotherapy using magnetic nanoparticles combined with external beam radiotherapy: Results of a feasibility study on patients with glioblastoma multiforme. J Neurooncol 2007;81:53–60.
14. Moghimi SM, Hunter AC, Murray JC. Nanomedicine: Current status and future prospects. FASEB J 2005; 19:311–330.
15. Chastellain M, Petri A, Gupta A, Rao KV, Hofmann H. Superparamagnetic silica-iron oxide nanocomposites for application in hyperthermia. Adv Eng Mater 2004;6:235–241.
16. Povlsen CO, Rygaard J. Heterotransplantation of human adenocarcinomas of colon and rectum to mouse mutant nude. A study of 9 consecutive transplantations. Acta Pathol Microbiol Scand A 1971;79:159–169.
17. Sun LQ, Vogel CA, Mirimanoff RO, Coucke P, Slosman DO, Mach JP, Buchegger F. Timing effects of combined radioimmunotherapy and radiotherapy on a human solid tumor in nude mice. Cancer Res 1997;57:1312–1319.
18. Sutherland R, Buchegger F, Schreyer M, Vacca A, Mach JP. Penetration and binding of radiolabeled anti-carcinoembryonic antigen monoclonal antibodies and their antigen binding fragments in human colon multicellular tumor spheroids. Cancer Res 1987;47:1627–1633.
19. Budden R, Kuhl UG, Buschmann G. Studies on pharmacodynamic activity of several drug solvents. 1. Diethyleneglycolmonoethylether, N,N-Diethylacetamide, Dimethylsulfoxide. Arzneimittelforschung 1978;28: 1571–1579.
20. Mottu F, Laurent A, Rüfenacht DA, Doelker E. Organic solvents for pharmaceutical parenterals and embolic liquids. A review of toxicity data. PDA J Pharm Sci Technol 2000;54:456–469.
21. Mottu F, Stelling MJ, Rüfenacht DA, Doelker E. Comparative hemolytic activity of undiluted organic water-miscible solvents for intravenous and intra-arterial injection. PDA J Pharm Sci Technol 2001;55:16–23.
22. Buchegger F, Haskell CM, Schreyer M, Scazziga BR, Randin S, Carrel S, Mach JP. Radiolabeled fragments of monoclonal antibodies against carcinoembryonic antigen for localization of human colon carcinoma grafted into nude mice. J Exp Med 1983;158:413–427.

23. Sutherland RM, Buchegger F, Schreyer M, Vacca A, Mach JP. Penetration and binding of radiolabeled anti-carcinoembryonic antigen monoclonal antibodies and their antigen binding fragments in human colon multicellular tumor spheroids. Cancer Res 1987;47:1627–1633.
24. Sutherland RM, Sordat B, Bamat J, Gabbert H, Bourrat B, Mueller-Klieser W. Oxygenation and differentiation in multicellular spheroids of human colon carcinoma. Cancer Res 1986;46:5320–5329.
25. Sapareto SA, Dewey WC. Thermal dose determination in cancer therapy. Int J Radiat Oncol Biol Phys 1984;10: 787–800.
26. Lepock JR. Cellular effects of hyperthermia: Relevance to the minimum dose for thermal damage. Int J Hyperthermia 2003;19:252–266.
27. Jordan O, Doelker E, Defabiani N, Caviezel A, Iselin C. Novel injectable urethral bulking agents for the treatment of urinary incontinence. J Mater Sci Mater Med 2004;15:519–522.
28. Bohner M. Theoretical considerations on the injectability of calcium phosphate cements. Proceedings of the 17th European Society for Biomaterials Conference, Barcelona, Spain, September 2002.
29. Bohner M, Baroud G. Injectability of calcium phosphate pastes. Biomaterials 2005;26:1553–1563.
30. Bernhardt JH, Brix G. Safety aspects of magnetic fields. In: Andra W and Nowak H, editors. Magnetism in Medicine. Weinheim: Wiley; 2007. pp 76–95.
31. Gellermann J, Wust P, Stalling D, Seebass M, Nadobny J, Beck R, Hege HC, Deuflhard P, Felix R. Clinical evaluation and verification of the hyperthermia treatment planning system HyperPlan. Int J Radiat Oncol Biol Phys 2000;47: 1145–1156.
32. Ivkov R, DeNardo SJ, Daum W, Foreman AR, Goldstein RC, Nemkov VS, DeNardo GL. Application of high amplitude alternating magnetic fields for heat induction of nanoparticles localized in cancer. Clin Cancer Res 2005;11: 7093s–7103s.
33. Wust P, Gneveckow U, Johannsen M, Bohmer D, Henkel T, Kahmann F, Sehouli J, Felix R, Ricke J, Jordan A. Magnetic nanoparticles for interstitial thermotherapy – Feasibility, tolerance and achieved temperatures. Int J Hyperthermia 2006;22:673–685.
34. Johannsen M, Gneveckow U, Thiesen B, Taymoorian K, Cho CH, Waldofner N, Scholz R, Jordan A, Loening SA, Wust P. Thermotherapy of prostate cancer using magnetic nanoparticles: Feasibility, imaging, and three-dimensional temperature distribution. Eur Urol 2006;52:1653–1662.
35. Johannsen M, Gneveckow U, Taymoorian K, Thiesen B, Waldofner N, Scholz R, Jung K, Jordan A, Wust P, Loening SA. Morbidity and quality of life during thermotherapy using magnetic nanoparticles in locally recurrent prostate cancer: Results of a prospective phase I trial. Int J Hyperthermia 2007;23:315–323.
36. Maier-Hauff K, Rothe R, Scholz R, Gneveckow U, Wust P, Thiesen B, Feussner A, von Deimling A, Waldoefner N, Felix R, et al. Intracranial thermotherapy using magnetic nanoparticles combined with external beam radiotherapy: Results of a feasibility study on patients with glioblastoma multiforme. J Neurooncol 2007;81:53–60.
37. Hilger I, Andra W, Hergt R, Hiergeist R, Schubert H, Kaiser WA. Electromagnetic heating of breast tumors in interventional radiology: In vitro and in vivo studies in human cadavers and mice. Radiology 2001;218:570–575.
38. Hilger I, Hiergeist R, Hergt R, Winnefeld K, Schubert H, Kaiser WA. Thermal ablation of tumors using magnetic nanoparticles – An in vivo feasibility study. Invest Radiol 2002;37:580–586.
39. Lyng H, Rofstad EK. Thermal dose and secondary tumour cell death. Int J Hyperthermia 1993;9:755–761.
40. Moroz P, Jones SK, Gray BN. The effect of tumour size on ferromagnetic embolization hyperthermia in a rabbit liver tumour model. Int J Hyperthermia 2002;18:129–140.
41. Andra W, d'Ambly CG, Hergt R, Hilger I, Kaiser WA. Temperature distribution as function of time around a small spherical heat source of local magnetic hyperthermia. J Magn Magn Mater 1999;194:197–203.
42. Rabin Y. Is intracellular hyperthermia superior to extracellular hyperthermia in the thermal sense? Int J Hyperthermia 2002;18:194–202.
43. Kolios MC, Worthington AE, Holdsworth DW, Sherar MD, Hunt JW. An investigation of the flow dependence of temperature gradients near large vessels during steady state and transient tissue heating. Phys Med Biol 1999;44: 1479–1497.
44. Hergt R, Andra W. Magnetic hyperthermia and thermoablation. In: Andra W and Nowak H, editors. Magnetism in Medicine. Weinheim: Wiley; 2007. pp 551–570.
45. Dewhirst MW, Sneed PK. Those in gene therapy should pay closer attention to lessons from hyperthermia. Int J Radiat Oncol Biol Phys 2003;57:597–599.
46. Hergt R, Andra W, d'Ambly CG, Hilger I, Kaiser WA, Richter U, Schmidt HG. Physical limits of hyperthermia using magnetite fine particles. IEEE Trans Magn 1998;34: 3745–3754.